Model Predictive Control for Luminous Flux Tracking in Light Emitting Diodes

Silvio Baccari *Member, IEEE,*, Francesco Vasca *Senior Member, IEEE,*, Massimo Tipaldi, and Luigi Iannelli *Senior Member, IEEE,*

***Abstract*—Luminous flux tracking and junction temperature stress minimization are typical objectives in the regulation of high-brightness Light Emitting Diodes (LEDs). In this paper a solution based on a Model Predictive Controller (MPC) approach is proposed. The state estimation is obtained by using a LED photoelectrothermal dynamic model whose parameters are tuned through a procedure here presented. By exploiting the dynamic separation within the thermal state variables of the model, the junction temperature is predicted by using LED current and heat sink temperature measurements. The effectiveness of the proposed approach is verified through simulations and experiments on different heat sinks and samples of the same LED family, thus confirming the achievement of the luminous flux tracking under current and temperature constraints typically featuring LED applications.**

***Index Terms*—Luminous flux tracking, light emitting diodes (LEDs), photoelectrothermal dynamic model, model predictive control, DC–DC buck converter.**

I. Introduction

LIGHT Emitting Diodes (LEDs) represent a promising solution for a wide spread replacement of the traditional lighting components with more efficient and flexible devices [1]–[4]. Different topologies and strategies have been proposed in the literature for the LED drivers design, among others see [5]–[7] and the references therein. Concisely one could say that there exist two approaches for defining the current that the LED driver should provide [8]: the LED current is controlled such that its average value provides the desired luminous flux, e.g. [9]–[11]; the instantaneous current produces an instantaneous illumination that is averaged by the human eye filtering capabilities thus providing the desired illumination [5], [12]. In both cases, the driver control problem consists in regulating the LED current to a reference trajectory. Nonetheless, it is not a trivial task to determine the LED driver reference signal able to provide the desired luminous flux by taking into account also the electrical and thermal constraints. Regardless of the current regulation strategy, the reference current is usually obtained by using a static map relating the luminous flux to the LED current. Yet the nonlinear dependence of the luminous efficacy on the device forward current presents a typical degradation for large currents [13], [14]. Moreover, the temperature also affects such nonlinear characteristic and a proper static and dynamic thermal management is a key factor for counteracting the undesired photometric variations [15].

The authors are with the Department of Engineering, University of Sannio, Piazza Roma 21, Benevento 82100, Italy (e-mail: silvio.baccari@unisannio.it; vasca@unisannio.it; mtipaldi@unisannio.it; luigi.iannelli@unisannio.it;)

The construction of a model which is able to capture and combine the luminous, the electrical and the thermal phenomena, i.e., a photoelectrothermal model, is a crucial preliminary step for the LED reference current design [16], [17]. Static models are analyzed, among others, in [14], [18], [19], while dynamics are taken into account in [20], [21]. The photoelectrothermal model here proposed is based on a one-dimensional thermal flow from the LED junction to the environment by using equivalent thermal resistors and capacitors [22], [23]. The dynamic separation among the thermal parts of the model is exploited in order to define a reduced-order model suitable for the controller design and implementation. Moving on from such models, the typical static characteristics can thus be interpreted as the steady-state behavior resulting from dynamic photoelectrothermal models [16], [20].

The proposed controller is characterized by two nested loops: the inner loop consists of a current controlled DC–DC buck power converter [5] while the outer loop provides the reference current to be tracked by the inner loop. In particular the outer loop consists of a Model Predictive Controller (MPC) aimed at regulating the LED luminosity by solving an optimization problem formulated on the reduced-order dynamic model. By exploiting the typical MPC features [24], [25], the proposed controller provides a unifying multi-variable system framework where objective functions based on the typical LED performances, e.g., luminosity, heating, electric efficiency, can be integrated and tuned according to the specific goals. In the presence of flux measurements it is possible to include the integral of the LED luminous flux error in the cost function and the proposed MPC can be interpreted as an extension of the most common sensor-based approaches with flux feedback and temperature feedforward compensations [26]. The proposed solution can be customized according to the design requirements, guarantees a wide operating range and, thanks to the above-mentioned extension, can counteract the LED aging process (usually faster than the one of the light sensors). Moreover, it allows to deal with constraints (e.g., current peak, maximum temperature), that can be handled during the control design phase. Finally, the computation of the control signal is based on an optimization procedure, which takes into account the desired reference trajectories for luminosity and temperature.

The rest of the paper is organized as follows. In Section II the photoelectrothermal LED model is derived. A procedure for the determination of the model parameters is presented in Section III. The MPC is described in Section IV. Numerical

and experimental results are given in Section V by considering different heat sinks and LED samples, and by comparing the good performances of the MPC with those achievable by a standard controller. Section VI concludes the paper.

II. Photoelectrothermal Model

It is well-known that the LED current, say i_f, gradually increases with the forward voltage, say v_f. This empirical observation gives the idea of modeling a LED as a diode connected to an equivalent series resistor, say R_d, resulting from the resistance of the p-n junction, contacts and current spreading layer [27]. Thus, the LED voltage–current characteristic can be modeled as

$$v_f(i_f, T_j) = \frac{n k_B T_0}{q} \left[1 - k_v \left(\frac{T_j}{T_0} - 1\right)\right] \ln\left(1 + \frac{i_f}{I_0}\right) + R_d i_f \tag{1}$$

where I_0 is the reverse saturation current, T_j the junction temperature, k_B the Boltzmann constant, q the electric charge, n the ideality factor, T_0 a nominal temperature and k_v a nonnegative constant used to represent the shift of the voltage–current characteristic for different values of the junction temperature [21], [28]. The thermal dependence of the characteristic is concentrated into the linear term depending on k_v and the saturation current is assumed to be constant.

The electric power supplied to the LED can be expressed as

$$P_{el}(i_f, T_j) = v_f(i_f, T_j)\, i_f \tag{2}$$

where the characteristic $v_f(i_f, T_j)$ is given by (1). A fraction of the electrical power supplied to the LED is transformed into the optical power. By assuming that the optical power P_{opt} and the electrical power P_{el} are measurable, one can define the so-called wall-plug efficiency [19]:

$$\eta_p \triangleq \frac{P_{opt}}{P_{el}}. \tag{3}$$

The definition (3) can be interpreted as an "external" efficiency because it is based on quantities that are directly measurable without considering any specific internal phenomena.

The power balance can be modeled by assuming that the total electric power determines the lighting effects and heating. Then, by using (3), one can write:

$$P_{el} = P_{opt} + P_{heat} = \eta_p P_{el} + (1 - \eta_p) P_{el}. \tag{4}$$

The efficiency η_p depends on both the junction temperature and the LED current. In the following we assume that the wall-plug efficiency is expressed by means of the bilinear function

$$\eta_p(i_f, T_j) = \bar{\eta}_p \left[1 - k_i \left(\frac{i_f}{I^*} - 1\right)\right] \left[1 - k_\eta \left(\frac{T_j}{T^*} - 1\right)\right], \tag{5}$$

where $\bar{\eta}_p$ is the efficiency at the nominal temperature $T_j = T^*$ and nominal current $i_f = I^*$. The nonnegative constants k_i and k_η are such that $0 < \eta_p(i_f, T_j) < 1$ for any i_f and T_j of interest. The bilinear model (5) is similar to the expression used in [14], [29] . It can be deduced from the characteristics reported in [19] and can be interpreted as a simplified version of the model adopted in [30]. The specific expression of the efficiency η_p is not crucial for the application of the methodology proposed in this paper, which can be applied for any reasonable nonlinear model of the wall-plug efficiency. The expression (5) is validated in Section III by considering the LED characteristic of luminous flux versus current for different temperatures, and it turns out to be in line with flux measurements through the calibration of the sensor used in the feedback so as shown in Section V-A.

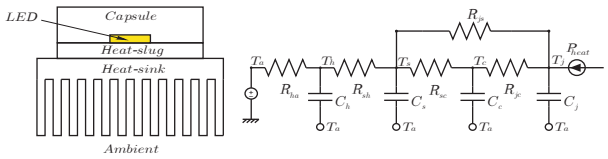

Fig. 1: Heat transfer equivalent scheme for a typical LED implementation.

In order to represent the dynamic thermal model, the following subscripts are defined: j for the junction, c for the capsule, s for the heat slug, h for the heat sink and a for the ambient. Denote by T the temperatures, assumed to be uniform in each part, m the equivalent masses, c the heat capacities. The symbols R indicate the equivalent thermal resistances and $C = mc$ the corresponding thermal capacitances, see Fig. 1.

By considering the (electrical) series connection of N_d LEDs that share only the common heat sink, the following dynamic model for the heat transfer can be derived by using the energy conservation principle:

$$m_j c_j \frac{dT_j}{dt} = \big(1 - \eta_p(i_f, T_j)\big) P_{el}(i_f, T_j) - \frac{1}{R_{jc}}(T_j - T_c) - \frac{1}{R_{js}}(T_j - T_s) \tag{6a}$$

$$m_c c_c \frac{dT_c}{dt} = \frac{1}{R_{jc}}(T_j - T_c) + \frac{1}{R_{sc}}(T_s - T_c) \tag{6b}$$

$$m_s c_s \frac{dT_s}{dt} = \frac{1}{R_{js}}(T_j - T_s) - \frac{1}{R_{sc}}(T_s - T_c) - \frac{1}{R_{sh}}(T_s - T_h) \tag{6c}$$

$$m_h c_h \frac{dT_h}{dt} = \frac{N_d}{R_{sh}}(T_s - T_h) - \frac{1}{R_{ha}}(T_h - T_a). \tag{6d}$$

The model (6) is linear with respect to P_{heat}, see (4), and nonlinear when the electrical current i_f is considered as an input. In particular (6a) is nonlinear due to the dependence of the wall-plug efficiency η_p and electric power P_{el} on the junction temperature. Moreover the LED current i_f is considered as an independent variable because it is directly controlled by the power converter which drives the LED.

The luminous flux Φ_v is clearly an output of interest for the model. To show how Φ_v is related to the thermal and electrical variables of the model, the luminous efficiency E of a light source is introduced and expressed as the product of the luminous efficacy of the optical radiation, E_r, and the power efficiency [17]:

$$E = \frac{\Phi_v}{P_{el}} = \frac{\Phi_v}{P_{opt}} \frac{P_{opt}}{P_{el}} = E_r\, \eta_p. \tag{7}$$

By considering a series connection of N_d LEDs and by using (7) one can write

$$\Phi_v(i_f, T_j) = N_d E_r \, \eta_p(i_f, T_j) \, P_{el}(i_f, T_j), \tag{8}$$

where the wall-plug efficiency η_p is given by (5) and the electrical power can be expressed as (2).

The computational load capabilities of the typical commercial digital controllers for LEDs make the model (6) too complex to be adopted for a real implementation. In order to overcome such issue, a reduced-order thermal model can be obtained from (6) by assuming

$$m_\xi c_\xi \ll m_h c_h \tag{9}$$

for any $\xi \in \{j, c, s\}$, i.e., the diode thermal capacities are negligible in comparison with the heat sink thermal capacity. The assumption (9) will be justified in Section III by exploiting the model parameters tuning procedure. At a slow time-scale one can assume that the small parameters $m_\xi c_\xi$ are zero, thus obtaining from (6a)–(6c) the corresponding equations at steady-state. By solving such equations, one can write the corresponding steady-state temperatures, say $\hat{T}_c$ and $\hat{T}_s$, as linearly dependent on the steady-state temperature $\hat{T}_j$ and the instantaneous temperature T_h, thus obtaining

$$0 = \alpha_1 \left(1 - \eta_p(i_f, \hat{T}_j)\right) P_{el}(i_f, \hat{T}_j) + \alpha_2 \hat{T}_j + \alpha_3 T_h, \tag{10}$$

where α_1, α_2 and α_3 are derived from (6a)–(6c) at steady-state:

$$\alpha_1 = 1 + \frac{R_{sh}}{R_{jc} + R_{sc}} + \frac{R_{sh}}{R_{js}}, \tag{11a}$$

$$\alpha_2 = \frac{R_{sc}}{R_{jc}(R_{jc} + R_{sc})} - \frac{1}{R_{jc}} - \frac{1}{R_{js}}, \tag{11b}$$

$$\alpha_3 = \frac{1}{R_{jc} + R_{sc}} + \frac{1}{R_{js}}. \tag{11c}$$

By considering (5) and (2) with (1), it is simple to deduce that (10) is quadratic in $\hat{T}_j$. For each pair (i_f, T_h) within realistic ranges, the equation (10) has two real solutions of different sign. Then, by considering the positive solution, one can conclude that (10) represents a unique mapping from (i_f, T_h) to $\hat{T}_j$.

By adding the equations (6a)–(6c) at steady-state, the dynamic equation (6d) can be rewritten as

$$m_h c_h \frac{dT_h}{dt} = N_d\big(1 - \eta_p(i_f, \hat{T}_j)\big) P_{el}(i_f, \hat{T}_j) - \frac{1}{R_{ha}}(T_h - T_a), \tag{12}$$

where $\hat{T}_j$ is constrained from (10) and can be analytically determined as a function of T_h and i_f by taking the positive solution of the quadratic equation (10). The model (12) corresponds to an equivalent electrical circuit which can be obtained from the one shown in Fig. 1 by solving it after assuming C_j, C_c and C_s to be zero, i.e., the corresponding capacitors replaced by open circuits. In particular, the heating power source P_{heat} is given by the state dependent function expressed by the first term in the right hand side of (12).

The model (12) with (10) and (5) will be used for the controller design and for its implementation in the experimental setup. The more complex model (6) will be used as the actual process model for the numerical validation.

III. Model Parameters Selection

In this section a procedure for the model parameters selection, starting from typical information reported in the LED datasheets and based on step-response experiments, is presented. The parameters are referred to the datasheet of the LED CREE family Xlamp Xp-G (product code XPGWHT-L1-0000-00CE7,). A procedure for the parameters determination of the complete model (6) and of the reduced-order model (12) is described. Note that only the latter one has to be identified for the controller implementation.

Table I reports all the parameters and physical constants (and their values) adopted in this paper. It already highlights whether they are already available (e.g. in the LED datasheets) or they need to be identified.

As regards the model (1) of the voltage–current LED characteristic, the nominal temperature is T_0, while $k_B =$ and q are physical constants. The parameters of (1) to be determined are n, I_0, R_d and k_v. The ideality factor n, the current I_0 and the equivalent resistance R_d are estimated through a linear regression approach applied by using the model (1) and the LED data at the nominal temperature (note that for $T_j = T_0$ the characteristic (1) does not depend on k_v). The parameter k_v can be computed from the information usually available from the LED datasheets, wherein the values of the forward-biased voltage at T_0 and $\bar{T}_j = T_0 + \Delta T_j$ are provided at a specific current test $\bar{i}_f$. By exploiting (1), it is straightforward to show that

$$k_v = -\frac{q \Delta v_f}{n k_B \Delta T_j \ln\left(1 + \frac{\bar{i}_f}{I_0}\right)} \tag{13}$$

where $\Delta v_f = v_f(\bar{i}_f, \bar{T}_j) - v_f(\bar{i}_f, T_0)$. The parameters identification for (8) must be completed by selecting the parameters $\bar{\eta}_p$, k_i and k_η of the efficiency expression (5). The values of the luminous flux Φ_v for different LED currents at the nominal temperature T^* can be deduced from the LED datasheets, see the stars in Fig. 2. Therefore, the nominal luminous efficiency $\bar{\eta}_p$ is calculated by exploiting (5) and (8) with $i_f = I^*$ and $T_j = T^*$. The parameter k_i is determined by using a least square (LS) algorithm to fit the model (8) with the LED datasheet values at $T_j = T^*$. The parameter k_η is evaluated from the LED datasheets, that is by using data on the luminous flux gradient versus the junction temperature T_j, at the nominal current $i_f = I^*$.

The luminous flux characteristics curves in Fig. 2, which present the typical concave shape discussed in the literature [13], allow to make considerations suitable for the luminous flux control. First of all it should be noticed that, by assuming a maximum current equal to $1.5\,\mathrm{A}$, at steady-state it is not possible to provide a luminous flux larger than approximatively $238\,\mathrm{lm}$, i.e. the maximum of the curve interpolating the filled circles. On the other hand larger fluxes are possible during transients. For instance starting from the steady-state point $(i_f, T_j) = (0.5\,\mathrm{A}, 335.4\,\mathrm{K})$ which corresponds to a luminous flux around $130\,\mathrm{lm}$, and by providing a current step till $1.5\,\mathrm{A}$, since the current dynamics are much faster than the thermal ones, the operating point will approximatively move on the characteristic at a constant temperature equal to

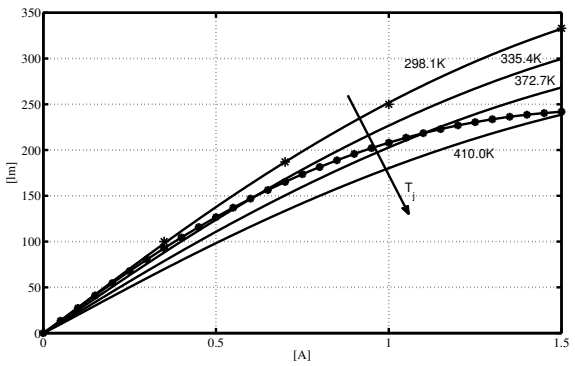

Fig. 2: Luminous flux Φ_v vs. current i_f for different junction temperatures: the stars indicate values from datasheet at $T_j = T^* = 298.1\,\mathrm{K}$; other curves represent (8) for different values of T_j; the filled circles (with the corresponding interpolating curve) indicate the luminous flux Φ_v calculated with (8) for different currents and T_j obtained from (6) at steady-state.

$T_j = 335.4\,\mathrm{K}$ by providing a luminous flux equal to $300\,\mathrm{lm}$. Then the operating point will change at a constant current equal to $1.5\,\mathrm{A}$, and the increasing of the junction temperature will reduce the luminous flux till the steady-state point is reached, i.e. $i_f = 1.5\,\mathrm{A}$, $T_j = 410\,\mathrm{K}$, $\Phi_v = 238\,\mathrm{lm}$. The best transient path from a given steady-state operating point to another one is not obvious and to this aim the MPC will show its potentialities. In order to complete the model parameters identification, the parameters of the dynamic equations must be determined. By taking into account the separation among the thermal dynamics, the most important thermal parameters are those characterizing the heat sink dynamics represented by the reduced-order thermal model (12). By considering the experimental setup described in Section V and by forcing the LED with a step variation of its current, the values of the parameters $m_h c_h$ and R_{ha} are selected so to provide a good fitting between the evolution predicted by the model (12) and the experimental data. The mass m_h is available from the datasheet. Finally, the values $m_j c_j$, $m_c c_c$, $m_s c_s$, and the thermal resistances R_{js}, R_{sh}, R_{jc} and R_{sc} are chosen coherently with similar models presented in the literature [20], [22], [31]. The identified values of the parameters confirm the validity of (9).

Symbol	Value	Source
m_j	$0.1\,\mathrm{g}$	See [20], [22], [31]
c_j	$0.49\,\mathrm{J\,g^{-1}\,K^{-1}}$	See [20], [22], [31]
c_c	$0.35\,\mathrm{J\,g^{-1}\,K^{-1}}$	”
c_s	$0.88\,\mathrm{J\,g^{-1}\,K^{-1}}$	”
c_h	$0.90\,\mathrm{J\,g^{-1}\,K^{-1}}$	Thermal capacity of aluminium
E_r	$248\,\mathrm{lm\,W^{-1}}$	Physical constant, see [32]–[35]
$\bar{\eta}_p$	0.38	Calculated by exploiting (5)
h_c	$15\,\mathrm{s}$	Control design choice
h_{PID}	$0.1\,\mathrm{ms}$	”
h_s	$1\,\mathrm{ms}$	”
h_{sim}	$2.7913 \times 10^{-6}\,\mathrm{s}$	”
k_B	$1.3807 \times 10^{-23}\,\mathrm{J\,K^{-1}}$	Physical constant
k_η	0.5168	LED datasheet
k_i	0.0935	LS when fitting data on model (8)
k_v	0.2278	Solving (13) from LED datasheet
I_0	$6.057 \times 10^{-11}\,\mathrm{A}$	Electronic devices literature
I^*	$350\,\mathrm{mA}$	Nominal current
m_c	$4.2 \times 10^{-3}\,\mathrm{g}$	Mass of epoxy hemisphere
m_s	$2.0\,\mathrm{g}$	See [20], [22], [31]
m_h	$40.0\,\mathrm{g}$	Heat sink datasheet
n	4.8756	Estimated form datasheet data
N_d	1	Experimental setup
q	$1.6022 \times 10^{-19}\,\mathrm{C}$	Physical constant
R_{sh}	$10\,\mathrm{K\,W^{-1}}$	See [20], [22], [31]
R_{ha}	$11.4\,\mathrm{K\,W^{-1}}$	”
R_{js}	$7\,\mathrm{K\,W^{-1}}$	”
R_{jc}	$70\,\mathrm{K\,W^{-1}}$	”
R_{sc}	$70\,\mathrm{K\,W^{-1}}$	”
R_d	$213\,\mathrm{m\Omega}$	Estimated form datasheet data
T_0	$298.15\,\mathrm{K}$	LED datasheet
T^*	$305.68\,\mathrm{K}$	Nominal temperature
T_a	$296.19\,\mathrm{K}$	Ambient temperature

TABLE I: Parameters and constants information source and values.

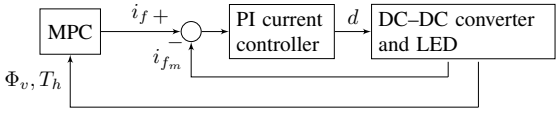

Fig. 3: Block scheme of the closed loop system: the outer feedback loop provides the reference current for an inner and faster LED current control loop which provides the duty cycle d to the power converter; i_{f_m} is the measured LED current and Φ_v is the measured LED flux.

IV. Model Predictive Controller

A block scheme of the proposed controller is shown in Fig. 3. Two nested loops are used. In the outer and slower loop the LED current i_f is considered as the control variable for an optimization problem constrained by the dynamics (12) together with the relation (10), which provide the prediction of the evolutions of the thermal state variables. The current computed by the MPC, say i_f, is the reference signal for an inner and faster control loop on the measured LED current.

The proposed MPC is obtained by solving a receding horizon optimization problem constrained by a discretized version of (10)–(12) and an integral controller of the LED luminous flux error, in the presence of flux measurements. The continuous dynamics (12) are discretized with a sampling period h_s and the constraints are active for each sampling time instant kh_s with k being a nonnegative integer. It is assumed that the controller requires a sampling period $h_c = N_s h_s > h_s$, with N_s being an integer, in order to compute a “good” suboptimal solution; without loss of generality, assume that the prediction horizon is given by $N_c h_c$ where N_c is a positive integer. In other words, the controller provides a sample of the control variable i_f each N_s integration cycles of the model, and the prediction horizon is a N_c-multiple of the controller sampling period h_c. By discretizing (12) with a forward technique and by using (10) the following expression can be obtained

$$T_h(k+1) = f_d\left(T_h(k), i_f(k), T_a\right) \tag{14}$$

where the state is the heat sink temperature whose samples are denoted by $T_h(k) = T_h(kh_s)$.

A further equation is included in the optimization problem,

which implements a controller on the integral of the flux error. In particular the following equation is considered

$$x_e(k+1) = x_e(k) + h_s\left(\Phi_v^{ref}(k) - \Phi_v(k)\right) \tag{15}$$

where Φ_v is the luminous flux and x_e is the new state variable corresponding to the cumulative flux error. The MPC can be formulated through the following optimization problem

$$\min_{i_f(\cdot)} \quad \left(\sum_{k=k_0}^{k_0+N} J_1(k) + \sum_{k=k_0}^{k_0+N-1} J_2(k) + \sum_{k=k_0+1}^{k_0+N+1} J_3(k)\right) \tag{16}$$

$$\begin{aligned}
\text{s.t.:} \quad & \text{model } (14)-(15) \text{ with } (10)\\
& i_f^{min} \le i_f(k) \le i_f^{max}\\
& T_j^{min} \le \hat{T}_j(k) \le T_j^{max}\\
& i_f(k_0+\nu+jN_s) = i_f(k_0+jN_s)\\
& \nu = 1,\dots,N_s-1, \quad j = 0,1,\dots,N_c-1
\end{aligned}$$

for $k = k_0,\dots,k_0+N$, $N = N_cN_s$, $\hat{T}_j(k)$ is given by (10) with $T_h = T_h(k)$ and $i_f = i_f(k)$. The cost functions are given by

$$\begin{aligned}
J_1(k) = \; & q_{T_j}\left(\hat{T}_j(k) - T_j^{ref}(k)\right)^2\\
& + q_{\Phi_v}\left(\Phi_v(k) - \Phi_v^{ref}(k)\right)^2, && \text{(17a)}\\
J_2(k) = \; & q_{i_f}(i_f(k) - i_f(k-N_s))^2, && \text{(17b)}\\
J_3(k) = \; & q_{x_e}x_e(k)^2, && \text{(17c)}
\end{aligned}$$

where the superscripts min, max and ref are used for indicating minimum, maximum and reference signals, respectively, of the corresponding variables, q_{T_j}, q_{Φ_v}, q_{i_f} and q_{x_e} are weighting parameters of the quadratic cost functions. In the last sum of (16), by considering (17c) and (15), the luminous flux $\Phi_v(k_0)$ is available from the last measurement while the remaining values $\Phi_v(k)$ for $k = k_0+1,\dots,k_0+N$ are predicted by using (8) with $T_j(k)$ given by the thermal model and $i_f(k)$ being the optimization variable. The equality constraints in the optimization problem (16) ensure that the controller output i_f is piecewise constant with a period equal to h_c. The term J_2 permits to reduce the variation of the control signal i_f in the prediction horizon. The term J_3 is useful when flux measurements are available and it introduces in the MPC formulation the action typical of a classical Proportional Integral (PI) controller. Indeed, by using $q_{x_e} \neq 0$ and thanks to (15), past and present flux errors are also weighted in the minimization problem. Instead, the LED luminous flux measurements do not affect the optimization problem solution when $q_{x_e} = 0$, because in this case the objective function depends only on model predictions.

The optimization problem (16) can be reformulated in order to include the temperature and current inequality constraints in the cost function. To this aim it is used a barrier function approach [36] which prescribes a high cost for violation of the constraints. The minimization problem (16) can be rewritten as

$$\begin{aligned}
\min_{i_f(\cdot)} \Bigg(& \sum_{k=k_0}^{k_0+N} J_1(k) + \sum_{k=k_0}^{k_0+N-1} J_2(k)\\
& + \sum_{k=k_0+1}^{k_0+N+1} J_3(k) + J_\varphi(k)\Bigg) && \text{(18)}\\
\text{s.t.:} \quad & \text{model } (14)-(15) \text{ with } (10)\\
& i_f(k_0+\nu+jN_s) = i_f(k_0+jN_s),\\
& \nu = 1,\dots,N_s-1, \quad j = 0,1,\dots,N_c-1
\end{aligned}$$

with $J_\varphi(k) = \mu_{i_f}\varphi_{i_f}(i_f(k_0), i_f(k_0+N_s),\dots,i_f(k_0+N)) + \mu_{T_j}\varphi_{T_j}(\hat{T}_j(k_0), \hat{T}_j(k_0+1),\dots,\hat{T}_j(k_0+N))$ where μ_{i_f} and μ_{T_j} are the weights of the barrier functions φ_{i_f} and φ_{T_j}. By substituting recursively (14), (15) and (8) in (18), the problem (18) can be rewritten in the following unconstrained form

$$\min_{i_f(\cdot)} \quad \widehat{\varphi}_{i_f}(i_f(k_0), i_f(k_0+N_s),\dots,i_f(k_0+N)), \tag{19}$$

which can be more easily implemented on a digital platform equipped with standard algorithms for multivariable function optimization.

V. Experiments

In this section the effectiveness of the proposed controller is verified through numerical and experimental results. The MPC implements (19). A comparison with a closed loop scheme similar to that in Fig. 3 where the MPC is replaced by a feedforward controller is provided.

A. Numerical and experimental setups

In the simulations the LED thermal model (6) together with the averaged model of the DC–DC buck power converter is used as the 'real' process to be controlled and it will be indicated as the photoelectrothermal model. The photoelectrothermal model with the MPC have been implemented on the Matlab/Simulink platform with four time-domains, each featured by a fixed integration time step. The first (and smallest) step size h_{sim} is chosen for the simulation of the photoelectrothermal model. The second sampling period $h_{PID} > h_{sim}$ is dedicated to the PI current controller which calculates the duty cycle on the basis of the error between the set point i_f provided by the MPC and the measured LED current. The third time step $h_s > h_{PID}$ is dedicated to the simulation of the thermal part of LED lamp inside the MPC optimization problem, while the last sampling period $h_c > h_s$ refers to the MPC. The PI controller sampling period is $h_{PID} = 0.1\,\text{ms}$. The step size for the model integration used by the MPC is $h_s = 1\,\text{ms}$, the MPC sampling period is $h_c = 15\,\text{s}$ and the length of the prediction horizon is $N_c = 10$. The PI parameters are 0.045 and 13.5 for the proportional and integral gains, respectively.

The experimental setup aims at verifying the performance of the proposed MPC. The setup follows the conceptual block scheme reported in Fig. 3. The inner control loop is based on

a PI current regulator which drives the power MOSFET of a DC–DC buck converter [37]. This regulator is implemented on a 32-bit micro-controller PIC32mx795f512l MCU, provided by Microchip. It receives the reference current (set every h_c seconds by the MPC) and provides the commands to the switch of the converter. The current measurement is obtained by a series resistor.

The MPC minimization problem (19) is implemented by means of the Real Time Windows Target toolbox and runs on a digital control platform based on Intel Core i7 processor at $3.4\,\mathrm{GHz}$. The reference current generated by the MPC is passed to the micro-controller by a serial port interface and in particular by the use of four bytes of data which are combined to obtain a 10 bits reference. The temperature measurements are forwarded to the MPC by means of the micro-controller board connected through the serial RS232. The heat sink temperature is measured by means of a sensor TMP05, which generates a modulated serial digital output that varies proportionally to the measured temperature. The LED luminous flux is measured by means of the light-to-frequency transducer TSL230. The light sensor is placed in correspondence of the maximum emitting flux direction according to the geometrical distributions of the luminous intensity provided by the LED and sensor datasheet. Dedicated flux measurement tests are carried out for the sensor calibration. An open loop test is done at a given current. The corresponding temperature is measured and the flux provided by the expression (8) is obtained. Then the sensor is calibrated, i.e., a proportional gain is determined and used as normalization factor during the experiments in order to make coherent the measured LED luminosity intensity with its flux values as provided by the datasheet at those operating conditions. The proposed implementation allows a conceptual validation of the approach, while an industrial/commercial realization should be achieved by embedded platforms and by calibration which considers the spectral responses of LED and sensor as well.

B. Luminous flux regulation

Let us consider a luminous flux regulation test case. The parameters of the cost function are $q_{T_h} = 0$, $q_{\Phi_v} = 100$, $q_{i_f} = 0$, $q_{x_e} = 0$, $\mu_{i_f} = \mu_{T_h} = 10^{-4}$. The maximum current is (also for the feedforward controllers) $i_f^{max} = 1\,\mathrm{A}$. The real time solution of the optimization problem is realized with a Matlab code which uses the fmincon method with the not scaled Sequential Quadratic Programming (SQP) algorithm and the following parameters: termination tolerances for the objective function TolFun $= 10^{-5}$ and for the state TolX $= 10^{-7}$, constraints tolerance TolCon $= 10^{-5}$, maximum number of function evaluations MaxFunEvals $= 100$, maximum number of iterations MaxIter $= 10$, lower bound of the objective limit ObjectiveLimit $= 10^{-3}$. The cost function (19) is implemented by using a logarithmic barrier function.

Figs. 4–5 show the experimental and simulation results (luminous flux and heat sink temperature, respectively) for the case of a luminous flux regulation to $200\,\mathrm{lm}$ obtained via the MPC and the feedforward controller. In accordance to what described above, the feedforward controller provides a reference current based on the nominal flux–current map, therefore the corresponding current is constant. Figs. 4–5 highlight a satisfactory consistency between experiments and numerical results as well as the coherence of the experimental steady-state with the maps presented in Fig. 2. The steady state flux difference between the MPC and the feedforward controller are due to the fact that the latter has no compensation of the measured temperatures. In order to show the performance of the MPC when the constraints are active, an experiment with the flux reference set to $220\,\mathrm{lm}$ has been carried out. The corresponding simulation and experimental results are reported in Fig.s 6–8.

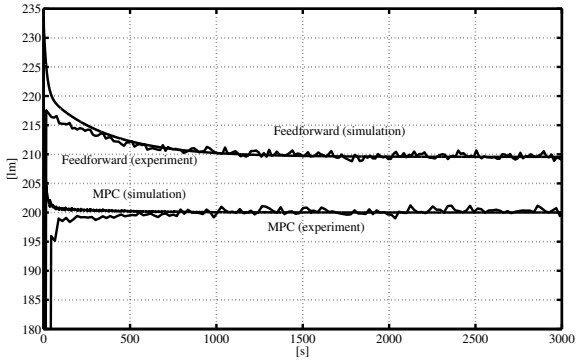

Fig. 4: Luminous fluxes obtained with the MPC and the feedforward controller in a luminous flux regulation test with $\Phi_v^{ref} = 200\,\mathrm{lm}$.

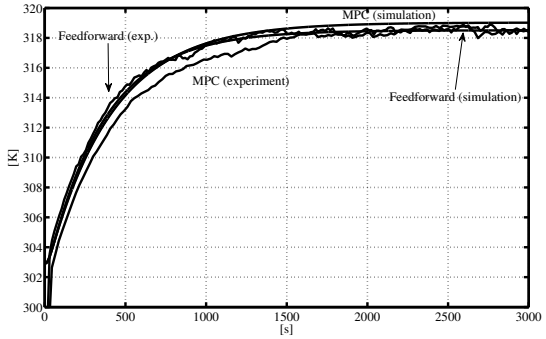

Fig. 5: Heat sink temperatures (same test of Fig. 4).

The quantitative (minor) differences between the simulations and experiments are due to the maximum number of iterations fixed for the experiments. The luminous flux is maintained at the maximum value compatible with the current and temperature constraints, see Fig. 6. The LED current evolution is due to the increase of the heat sink temperature, see Fig. 7, and it saturates at i_f^{max}. At around $800\,\mathrm{s}$ the current starts decreasing because the junction temperature becomes close to its maximum value which for this experiments has been set to $355\,\mathrm{K}$ (see Fig. 8). The (low amplitude) "spikes" of the simulated current are due to the very small difference between the simulated junction temperature and its maximum value.

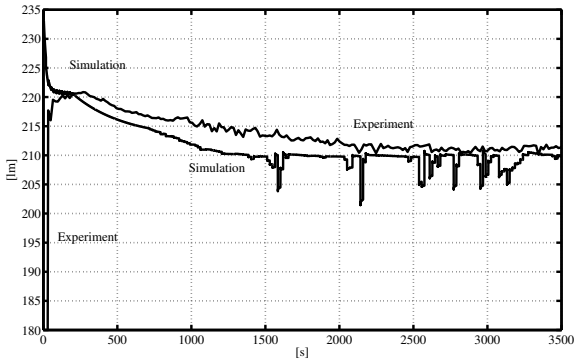

Fig. 6: Experimental and simulation results for the MPC in luminous flux regulation test with $\Phi_v^{ref} = 220\,\mathrm{lm}$.

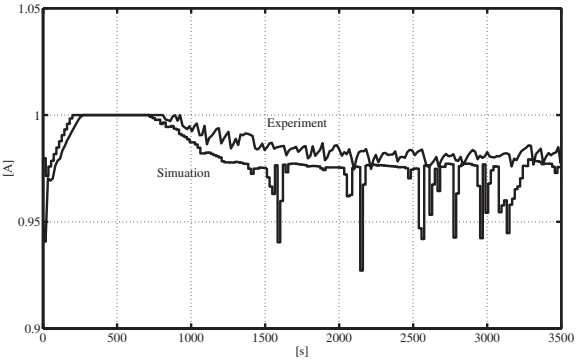

Fig. 7: LED currents for the same test of Fig. 6.

C. Different reference signals

Table II shows a comparison of the feedforward controller and MPCs for different cost functions. In particular the reference current of the feedforward controller is obtained via the steady-state map reported in Fig. 2 (filled circles with the corresponding interpolating curve) by using as entry the reference flux. The reference current of the feedforward controller is obtained via the steady-state map reported in Fig. 2 (filled circles with the corresponding interpolating curve) by using as entry the reference flux. Each column corresponds to a different value of the reference flux Φ_v^{ref}. The variables reported are the steady state junction temperature T_j^{ss}, the flux steady state error e_Φ^{ss} with respect to the reference flux, the steady state wall plug efficiency η_p^{ss}, the average value η^{int} over the simulation time interval of the difference between the instantaneous and the steady state wall plug efficiency (the highest the better), and the average value e_Φ^{int} over the simulation time interval of the flux error. Inspired by Fig. 8 the reference signal for the junction temperature, when used, is a piecewise linear signal starting from the initial value of the temperature with two breaking time-temperature points at $(500\,\mathrm{s}, 0.9T_j^{ss})$ and $(1500\,\mathrm{s}, T_j^{ss})$.

Var	Control	50 lm	100 lm	150 lm	200 lm	250 lm
T_j^{ss}	FF	306.13	315.92	328.43	345.98	379.39
	MPC_0	306.12	315.89	328.40	345.89	378.95
	MPC_1	306.12	315.62	328.42	344.89	375.68
	MPC_2	306.12	315.89	328.42	345.76	377.14
e_Φ^{ss}	FF	0.11	0.42	0.93	2.08	4.40
	MPC_0	0.01	0.04	0.11	0.24	0.56
	MPC_1	3.46	6.93	12.74	11.95	12.74
	MPC_2	0.06	0.17	1.83	0.70	1.83
η_p^{ss}	FF	0.40	0.37	0.34	0.31	0.24
	MPC_0	0.40	0.37	0.34	0.31	0.24
	MPC_1	0.40	0.37	0.34	0.31	0.25
	MPC_2	0.40	0.37	0.34	0.31	0.25
η^{int}	FF	0.0004	0.0008	0.0013	0.0019	0.0027
	MPC_0	0.0004	0.0010	0.0018	0.0033	0.0089
	MPC_1	0.0018	0.0035	0.2640	0.0084	0.0141
	MPC_2	0.0005	0.0011	0.2569	0.0037	0.0088
e_Φ^{int}	FF	0.1147	0.4207	0.9280	2.0775	4.4019
	MPC_0	0.0100	0.0426	0.1099	0.2395	0.5556
	MPC_1	3.4584	6.9283	48.8846	11.9483	12.7353
	MPC_2	0.0589	0.1657	0.2863	0.6992	1.8309

TABLE II: Comparison of the feedforward controller (FF) and MPCs with different cost functions: MPC_0 is with luminous flux tracking and $q_{T_h} = 0$; MPC_1 is with $q_{\Phi_v} = 0$ and temperature tracking; MPC_2 is with temperature and luminous flux tracking signals.

The MPC_0 performs always better than the feedforward one. The results of MPC_1 show the importance of considering the flux error in the cost function. By comparing the values of η^{int} corresponding to MPC_2 and MPC_0 at $\Phi_v^{ref} = 150\,\mathrm{lm}$ it is evident that the use of a reference temperature signal in the cost function can provide better performance when the luminous flux reference value correspond to intervals where the nonlinearity of the flux–current characteristic is more evident, see Fig. 2.

The effectiveness of the MPC non constant flux reference signals has been confirmed by experimental results in Fig. 9, for which a sinusoidal flux reference signal has been chosen.

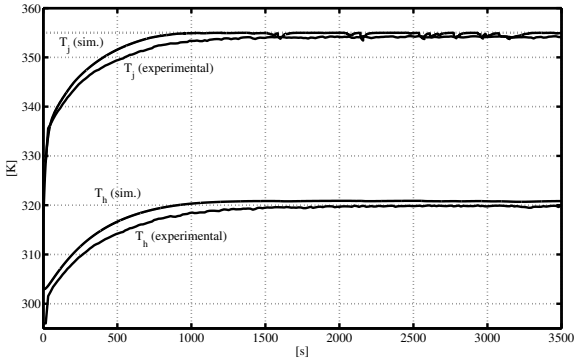

Fig. 8: Junction and heat sink temperatures for the same test of Fig. 6.

D. Different LEDs and heat sinks

In order to analyze the robustness of the proposed MPC tracking capability and performance a luminous flux regulation test with $\Phi_v^{ref} = 150\,\mathrm{lm}$ has been repeated for three different setups. The setup indicated by exp1 is the nominal plant used for the parameters tuning while exp2 and exp3 are featured by different LED pads and a different type of heat sink (exp3). In all three setups, the same MPC designed for the nominal case

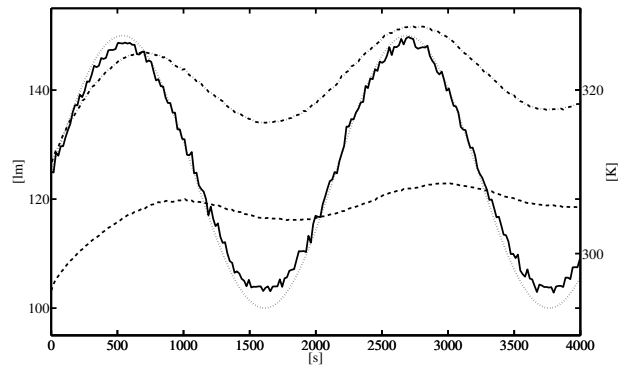

Fig. 9: Measured luminous flux (continuous line) with time varying reference flux (dotted line) obtained by adding a constant ($125\,\mathrm{lm}$) to a sinusoid (period equal to 36 minutes and amplitude equal to $25\,\mathrm{lm}$). The dashed and dot-dashed lines indicate the estimated junction temperature and the measured heat sink temperature, respectively.

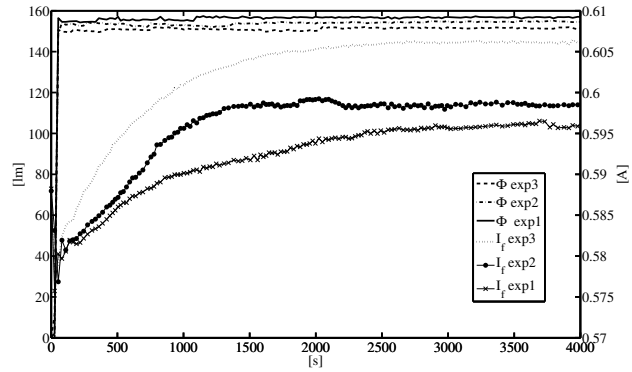

Fig. 10: LEDs currents and luminous fluxes for the three experimental setups and for a flux regulation test with $\Phi_v^{ref} = 155\,\mathrm{lm}$. For flux, continuous line represents the nominal case. Different values of the current are due to different values of the junction temperatures

has been adopted. The results of the experiments are shown in Fig 10.

Good reference flux regulations are obtained also in the not nominal scenario. The LED currents show how the MPC can compensate for the LED efficiency reduction due to the different evolutions of the heat sink temperature, independently from the ambient temperature.

E. Lookup table implementation

The solution of minimization problem (19) can be approximated by discretizing the flux and the heat sink temperature in a certain interval. In Fig. 11, the minimization problem has been uniformly discretized with a 30-step grid over the interval $[262.15\,\mathrm{K},\ 379.9\,\mathrm{K}]$ for T_h and $[10\,\mathrm{lm}\text{-}240\,\mathrm{lm}]$ for Φ_v^{ref}. The off-line calculated values are stored into a two dimensional array and can be accessed by a simple indexing operation. For a microcontroller retrieving a value from memory is faster

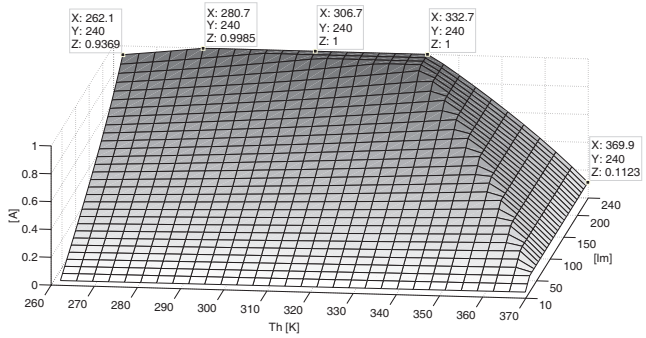

Fig. 11: Plot of $i_f(k_0)$ (Z-axis) which solve the problem (16) with constant reference luminous flux values (Y-axis) and heat sink temperature (X-axis).

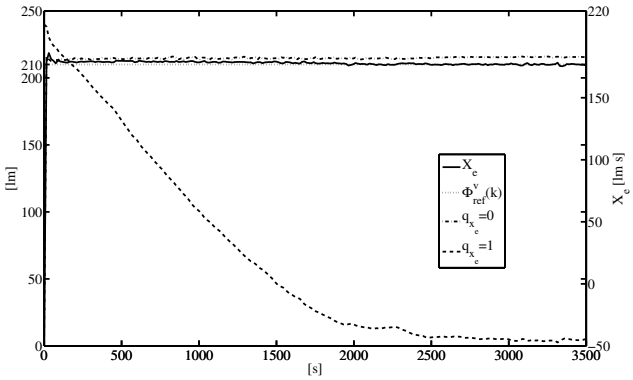

Fig. 12: Evolution of $x_e(k)$ and LED luminous flux measurement in the luminous flux feedback experiments with $q_{x_e} = 1$ and $q_{x_e} = 0$ for $\Phi_{ref}(k) = 210\,\mathrm{lm}$, and $q_{T_h} = 0$, $q_{\Phi_v} = 100$, $q_{i_f} = 0$, $\mu_{i_f} = \mu_{T_h} = 10^{-4}$.

than the on-line minimization procedure that can be executed on a powerful PC. The table is precalculated with a better precision (in this off line optimization maximum execution time constraints are not used) than the on-line computation and can be either implemented in the source code or stored in static memory support/ASIC hardware according to the specific application needs. The pre-computed values of i_f correspond to the first sample of the current in the control horizon with a constant reference flux. During the operating phase, the micro-controller can retrieve the LED reference forward current based on the measured T_h and the desired luminous flux value. The map in Fig. 11 provides results which are coherent with the experimental data in Fig. 10.

F. LED luminous flux feedback

The last experiment verifies the MPC performance in the presence of luminous flux measurements, i.e., with a nonzero term J_3 in (16). The experimental results in Fig. 12 show that, after a transient, a zero steady state error on the luminous flux is obtained, which is confirmed also by the constant steady state value of the state variable x_e.

VI. Conclusion

A model predictive controller (MPC) for LEDs modeled by a set of equations capturing their electric, thermal and optical behaviors has been presented. The proposed approach offers a comprehensive control framework, where different and conflicting objectives are handled simultaneously and extends the most common sensor-based approaches based on flux feedback and temperature feedforward compensation. In particular, the control strategy is capable of optimizing performance related to luminosity by satisfying the typical constraints on temperature and current. Simulation and experimental results demonstrate the effectiveness of the proposed control strategy which allows to obtain high wall plug efficiencies for luminous flux regulation problems also during transients when the constraints on critical process variables become active. A lookup table controller implementation has shown its practicality also for digital control platforms whose computational capabilities do not allow the online solution of the optimization problem.

References

[1] B. Bowers, "Lights out," IEEE Spectrum, vol. 48, no. 4, pp. 44–52, 2011.

[2] D. Tran and Y. K. Tan, "Sensorless illumination control of a networked led-lighting system using feedforward neural network," Industrial Electronics, IEEE Trans. on, vol. 61, no. 4, pp. 2113–2121, 2014.

[3] M. G. Craford, R. D. Dupuis, M. Feng, F. A. Kish, and J. Laskar, "50th Anniversary of the Light-Emitting Diode (LED): An Ultimate Lamp," Proc. of the IEEE, vol. 101, no. 10, pp. 2154–2157, 2013.

[4] S. Scalzi, S. Bifaretti, and C. Verrelli, "Repetitive learning control design for led light tracking," Control Systems Technology, IEEE Trans. on, vol. PP, no. 99, pp. 1–1, 2014.

[5] S. C. Tan, "General n-level driving approach for improving electrical-to-optical energy-conversion efficiency of fast-response saturable lighting devices," Industrial Electronics, IEEE Trans. on, vol. 57, no. 4, pp. 1342–1353, 2010.

[6] F. J. Azcondo, J. M. Alonso, and S. Y. R. Hui, "Special section on modern ballast technology and lighting applications," Industrial Electronics, IEEE Trans. on, vol. 59, no. 4, pp. 1689–1759, 2012.

[7] M. S. Lin and C. L. Chen, "An integrated lighting unit with regulated pulse current driving technique," Industrial Electronics, IEEE Trans. on, vol. 60, no. 10, pp. 4694–4701, 2013.

[8] L. Yu-Liang, C. Huang-Jen, L. Yu-Kang, and L. Chung-Ming, "Led backlight driver circuit with dual-mode dimming control and current-balancing design," Industrial Electronics, IEEE Trans. on, vol. 61, no. 9, pp. 4632–4639, Sept 2014.

[9] X. Lv, K. Loo, Y. Lai, and C. Tse, "Energy-saving driver design for full-color large-area led display panel systems," Industrial Electronics, IEEE Trans. on, vol. 61, no. 9, pp. 4665–4673, Sept 2014.

[10] D. G. Lamar, M. Arias, A. Rodriguez, A. Fernandez, M. M. Hernando, and J. Sebastian, "Design-oriented analysis and performance evaluation of a low-cost high-brightness led driver based on flyback power factor corrector," Industrial Electronics, IEEE Trans. on, vol. 60, no. 7, pp. 2614–2626, 2013.

[11] X. Wu, C. Hu, J. Zhang, and C. Zhao, "Parallel autoregulated charge-balancing rectifier for multioutput light-emitting diode driver," Industrial Electronics, IEEE Trans. on, vol. 61, no. 3, pp. 1262–1268, March 2014.

[12] X. Lv, K. H. Loo, Y. M. Lai, and C. K. Tse, "Energy-saving driver design for full-color large-area led display panel systems," Industrial Electronics, IEEE Trans. on, vol. PP, no. 99, to appear.

[13] K. H. Loo, W. K. Lun, S. C. Tan, Y. M. Lai, and C. K. Tse, "On driving techniques for LEDs: Towards a generalized methodology," Power Electronics, IEEE Trans. on, vol. 24, no. 12, pp. 2967–2976, 2009.

[14] V. C. Bender, F. Mendes, N. Barth, W. D. Vizzotto, M. A. D. Costa, R. N. do Prado, and T. B. Marchesan, "An optimized methodology for LED lighting systems designers: A photometric analysis," in Proc. of IEEE Industrial Electronics Society Annual Conference, Montreal, Canada, Oct. 2012, pp. 4521–4526.

[15] P. Pickering, "Towards a systematic methodology for the design, testing and manufacture of high brightness light emitting diode lighting luminaires," Ph.D. dissertation, University of Manchester, 2013.

[16] S. Y. R. Hui, H. Chen, and X. Tao, "An extended photoelectrothermal theory for LED systems: A tutorial from device characteristic to system design for general lighting," Power Electronics, IEEE Trans. on, vol. 27, no. 11, pp. 4571–4583, 2012.

[17] V. Bender, O. Iaronka, W. Dotto Vizzotto, M. Dalla Costa, R. Nederson do Prado, and T. Bandeira Marchesan, "Design methodology for light-emitting diode systems by considering an electrothermal model," Electron Devices, IEEE Trans. on, vol. 60, no. 11, pp. 3799–3806, 2013.

[18] S. Y. R. Hui and Y. X. Qin, "A general photo–electro–thermal theory for light emittind diodes (LED) systems," Power Electronics, IEEE Trans. on, vol. 24, no. 8, pp. 1967–1976, 2009.

[19] A. Poppe and C. J. M. Lasance, "On the standardization of thermal characterization of LEDs," in Proc. of the 25th IEEE Semiconductor Thermal Measurement and Management Symposium, San Jose, CA, USA, March 2009, pp. 151–158.

[20] X. Tao and S. Y. R. Hui, "Dynamic photoelectrothermal theory for light-emitting diode systems," Industrial Electronics, IEEE Trans. on, vol. 59, no. 4, pp. 1751–1759, 2012.

[21] A. Poppe and T. Temesvölgyi, "A general multi-domain LED model and its validation by means of ac thermal impedance," in Proc. of IEEE Symposium on Semiconductor Thermal Measurement and Management, San Jose, California, USA, Mar. 2013, pp. 137–142.

[22] X. Tao and D. Zhang, "Thermal parameter extraction method for light-emitting diode (LED) systems," Electron Devices, IEEE Trans. on, vol. 60, no. 6, pp. 1931–1937, 2013.

[23] X. Tao, H. Chen, S. N. Li, and S. Y. R. Hui, "A new noncontact method for the prediction of both internal thermal resistance and junction temperature of white light-emitting diodes," Power Electronics, IEEE Trans. on, vol. 27, no. 4, pp. 2184–2192, 2012.

[24] Y. Wang and S. Boyd, "Fast model predictive control using online optimization," Control Systems Technology, IEEE Trans. on, vol. 18, no. 2, pp. 267–278, 2010.

[25] J. S. A. Carneiro and L. Ferrarini, "Preventing thermal overloads in transmission circuits via model predictive control," Control Systems Technology, IEEE Trans. on, vol. 18, no. 6, pp. 1406–1412, 2010.

[26] C.-W. Tang, B.-J. Huang, and S.-P. Ying, "Illumination and color control in red-green-blue light-emitting diode," Power Electronics, IEEE Trans. on, vol. 29, no. 9, pp. 4921–4937, 2014.

[27] J. Park and C. Lee, "An electrical model with junction temperature for light-emitting diodes and the impact on conversion efficiency," IEEE Electron Device Letters, vol. 26, no. 5, pp. 308–310, 2005.

[28] D. Gacio, J. M. Alonso, J. Garcia, M. S. Perdigao, E. S. Saraiva, and F. E. Bisogno, "Effects of the junction temperature on the dynamic resistance of white LEDs," Industry Applications, IEEE Trans. on, vol. 49, no. 2, pp. 750–760, 2013.

[29] P. Almeida, V. Bender, H. Braga, M. Dalla Costa, T. Marchesan, and J. Alonso, "Static and dynamic photoelectrothermal modeling of led lamps including low-frequency current ripple effects," Power Electronics, IEEE Trans. on, vol. 30, no. 7, pp. 3841–3851, 2015.

[30] H. Chen and S. Y. Hui, "Dynamic prediction of correlated color temperature and color rendering index of phosphor-coated white light-emitting diodes," Industrial Electronics, IEEE Trans. on, vol. 61, no. 2, pp. 784–797, 2014.

[31] T. Liuxi, L. Jia, K. Wang, and S. Liu, "Effects of defects on the thermal and optical performance of high-brightness light-emitting diodes," Electronics Packaging Manufacturing, IEEE Trans. on, vol. 32, no. 4, pp. 233–240, 2009.

[32] E. Schubert, Light-Emitting Diodes. Cambridge: Cambridge University Press, 2006.

[33] Y.-S. Tyan, "Organic light-emitting-diode lighting overview," Journal of Photonics for Energy, vol. 1, no. 1, pp. 011 009–011 009–15, 2011.

[34] Y. Ohno, "Spectral design considerations for white led color rendering," Optical Engineering, vol. 44, no. 11, pp. 111 302–111 302–9, 2005.

[35] T. W. Murphy Jr, "Maximum spectral luminous efficacy of white light," Journal of Applied Physics, vol. 111, no. 10, p. 104909, 2012.

[36] S. Baccari, L. Iannelli, and F. Vasca, "A parallel algorithm for implicit model predictive control with barrier function," in Proc. of IEEE Multi-Conference on Systems and Control, Dubrovnik, Croatia, Oct. 2012, pp. 1405–1410.

[37] F. Vasca and L. Iannelli, Eds., Dynamics and Control of Switched Electronic Systems. London, UK: Springer, 2012.